AJNR

Quantitative MRI in Multiple Sclerosis: From Theory to Application

M. Tranfa, G. Pontillo, M. Petracca, A. Brunetti, E. Tedeschi, G. Palma and S. Cocozza

AJNR Am J Neuroradiol 2022, 43 (12) 1688-1695
doi: https://doi.org/10.3174/ajnr.A7536
http://www.ajnr.org/content/43/12/1688

Quantitative MRI in Multiple Sclerosis: From Theory to Application

M. Tranfa, G. Pontillo, M. Petracca, A. Brunetti, E. Tedeschi, G. Palma, and S. Cocozza

ABSTRACT

SUMMARY: Quantitative MR imaging techniques allow evaluating different aspects of brain microstructure, providing meaningful information about the pathophysiology of damage in CNS disorders. In the study of patients with MS, quantitative MR imaging techniques represent an invaluable tool for studying changes in myelin and iron content occurring in the context of inflammatory and neurodegenerative processes. In the first section of this review, we summarize the physics behind quantitative MR imaging, here defined as relaxometry and quantitative susceptibility mapping, and describe the neurobiological correlates of quantitative MR imaging findings. In the second section, we focus on quantitative MR imaging application in MS, reporting the main findings in both the gray and white matter compartments, separately addressing macroscopically damaged and normal-appearing parenchyma.

ABBREVIATIONS: bSSFP = balanced steady-state free precession; CL = cortical lesions; GRE = gradient recalled-echo; NAWM = normal-appearing white matter; PD = proton density; qMRI = quantitative MR imaging; QSM = quantitative susceptibility mapping; RF = radiofrequency

While conventional MR imaging plays an unquestionable role in the diagnosis and management of MS,[1,2] it offers very limited information about the pathophysiology of tissue damage because conventional sequences are not able to detect subtle changes affecting WM and GM. Quantitative MR imaging (qMRI) bridges this gap, detecting brain microstructural alterations with high sensitivity and robustness to interscanner and interobserver variability, thus providing measures that can be compared among sites and longitudinal examinations. Furthermore, this technique has been successfully used to differentiate MS from other demyelinating diseases, such as neuromyelitis optica, which presents a different spectrum of relaxometry alterations[3] and a peculiar spatial deep gray matter involvement,[4] and also to characterize other conditions with different etiologies, from vascular disease to brain tumors.[5,6] However, the applications of qMRI extend beyond the brain, being able to depict changes in liver iron concentration[7] as well as the presence of fibrosis,[8] and prostatic calcifications,[9] and to evaluate cortical bone mineral density[10] or myocardial structural alterations.[11]

Although the definition of qMRI is open to different interpretations, several advanced MR imaging techniques are usually grouped under this umbrella, including relaxometry, magnetic susceptibility, diffusion invariants, magnetization transfer, and, to some extent, perfusion parameters.[12] Each of these techniques offers different, sometimes complementary, insights into the complex tissue alterations occurring in MS.[13] In this light, it is noteworthy to remember that, while demyelination represents the end result of a complex phenomenon of inflammation, ultimately leading to axonal and neuronal degeneration, change in iron homeostasis is a crucial step in the pathophysiology of damage in MS, linked to microglial activation and modifications in oligodendrocyte functionality.[14,15] Relaxometry plays a unique role, given that most of the above-mentioned qMRI techniques offer valuable and sensitive tools in myelin assessment but they lack iron-detection sensitivity. Indeed, relaxometry assesses abnormalities of iron and myelin, elements that are at the crossroads of the inflammatory and neurodegenerative components in MS pathophysiology.[12]

In this review, we summarize the role and the application of qMRI techniques, here defined as relaxometry (estimating R1, R2, R2*, and, by extension, proton density [PD]) and quantitative susceptibility mapping (QSM), to the study of patients with MS.

In the first section, we briefly describe the physics behind qMRI, together with its neurobiological correlates. In the second

Received January 12, 2022; accepted after revision February 22.

From the Departments of Advanced Biomedical Sciences (M.T., G. Pontillo, A.B., E.T., S.C.), and Electrical Engineering and Information Technology (G. Pontillo), University of Naples "Federico II," Naples, Italy; Department of Human Neurosciences (M.P.), Sapienza University of Rome, Rome, Italy; and Institute of Nanotechnology (G. Palma), National Research Council, Lecce, Italy.

Please address correspondence to Giuseppe Pontillo, MD, Department of Advanced Biomedical Sciences, University "Federico II," Via Pansini, 5, 80131 Naples, Italy; e-mail: giuseppe.pontillo@unina.it; @NeuroN_Lab

http://dx.doi.org/10.3174/ajnr.A7536

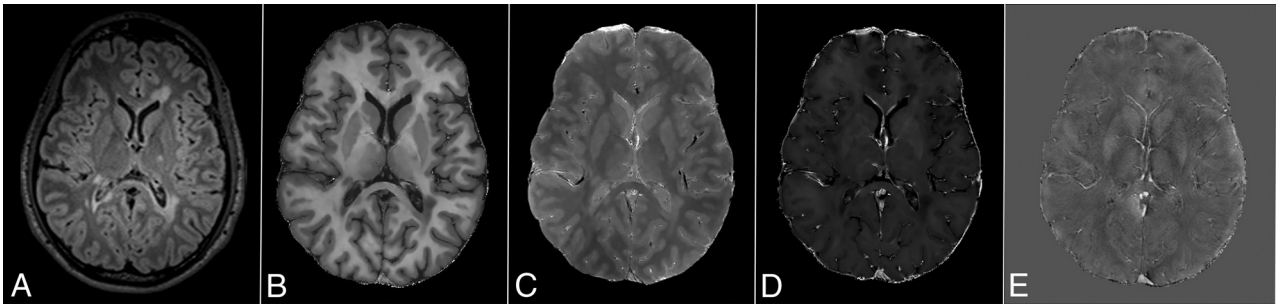

FIG 1. An example of quantitative MR imaging maps. Along with findings of a conventional FLAIR sequence (*A*) are examples of R1 (*B*), PD (*C*), R2* (*D*), and QSM (*E*) maps from a 22-year-old man with MS.

section, we summarize brain qMRI findings in MS for both the normal-appearing parenchyma and lesions in the GM and WM compartments.

qMRI Theory

Impact of Excitation Pulses and Significance of 3D Sequences. The R1 and R2 relaxation rates, defined as the inverses of T1 and T2 relaxation times, measure the efficiency of the kinetics mechanisms restoring the thermal equilibrium of the longitudinal and transverse components of the spin isochromats. An isochromat represents the magnetic moment associated with a subset of nuclei (protons, for our purposes) whose cardinality is large enough to justify a classic description of its dynamics (in terms of the expectation value of the quantum magnetic moment operator) and whose spatial extent is small enough to assume a strictly uniform macroscopic magnetic field throughout the subset. The evolution of the isochromats in an MR imaging sequence (radiofrequency [RF] and gradient pulses) is strongly dependent on the flip angles they experience. This shows why accurate R1 and R2 mapping is only possible through 3D sequences, which, unlike 2D sequences, guarantee a roughly uniform RF excitation throughout each voxel.

Estimation of Quantitative Maps. In general, the viable protocols for R1 and R2 mapping in neuroimaging routine rely on the acquisition of multiple 3D spoiled gradient recalled echo (GRE, for R1) and balanced steady-state free precession (bSSFP, for the additional information required to estimate R2) sequences at variable flip angles.[16] However, several aspects need to be considered to obtain accurate relaxation maps. First, nonideal slab profiles can be accounted for with a dedicated sequence for flip angle mapping[17] or through an iterative approach based on the information content of the estimated relaxation maps.[18] The bias from nonideal RF spoiling can be removed according to the specific phase increment implemented by each vendor.[19] Finally, to factor out the effects of off-resonance phenomena impacting the bSSFP images in the form of banding artifacts, one needs to adopt a modified version of the original bSSFP approach,[18] based on a synthetic contrast from multiple phase-cycled bSSFP.[20]

The estimation of the free induction decay rate (R2*) is comparatively simpler because it depends only on the ratios of the signals at different TEs, with no RF pulses in between. It is usually obtained through a multi-GRE sequence with flip angles close to the Ernst angle for SNR convenience and, therefore, can be estimated on the basis of the same protocol structure adopted for R1 mapping.[21]

Once R1 and R2* (which rule the signal equation of the spoiled GRE sequence) have been obtained, PD is ideally obtained without further acquisitions. Nevertheless, the spatial sensitivity of the receiver coil for the brain is substantially inhomogeneous; therefore, an additional low-resolution acquisition of one of the sequences with the body coil helps to mitigate the inhomogeneity bias.[22]

Finally, the phase of the complex images acquired for R2* mapping permits QSM.[23] The raw phase is first unwrapped and then filtered to remove the background component that is not associated with the local magnetization induced in the parenchyma by the main magnetic field.[24] The filtered phase is finally processed to solve the inverse problem leading to the QSM.[5] In this step, special care must be taken to avoid the occurrence of streaking artifacts that could impact the clinical value of the image by mimicking spurious anatomic structures (Fig 1).

Importance of Denoising Schemes. The mathematic problems associated with the qMRI protocols are typically ill-conditioned, thus leading to a detrimental noise propagation from the acquired images to the reconstructed maps. Therefore, besides the customary optimization of the acquisition protocol to maximize the SNR of the quantitative maps, a denoising step is warranted upstream of the qMRI pipeline. In this context, multispectral versions of the non-local means algorithms have been devised to account for the power distribution of noise in parallel imaging and to reconstruct the true signal from the raw statistical moments of the acquired images.[25,26]

Pathophysiologic Correlates of qMRI. The pathophysiology of brain damage in MS is multifaceted, being characterized by a sequence of demyelination and partial remyelination events associated with neurodegeneration.[27]

Microglia activation within normal-appearing WM (NAWM) is one of the earliest and most prominent features in MS pathophysiology.[28] Subsequently, a loss of integrity of the blood-brain barrier, driven by proinflammatory mediators produced by resident and endothelial cells, as well as indirect leukocyte-dependent damage,[27] leads to focal demyelination. As the disease progresses, oligodendrocyte depletion occurs,[29] as well as oligodendroglial iron release,[30] secondary to the high concentration of proinflammatory

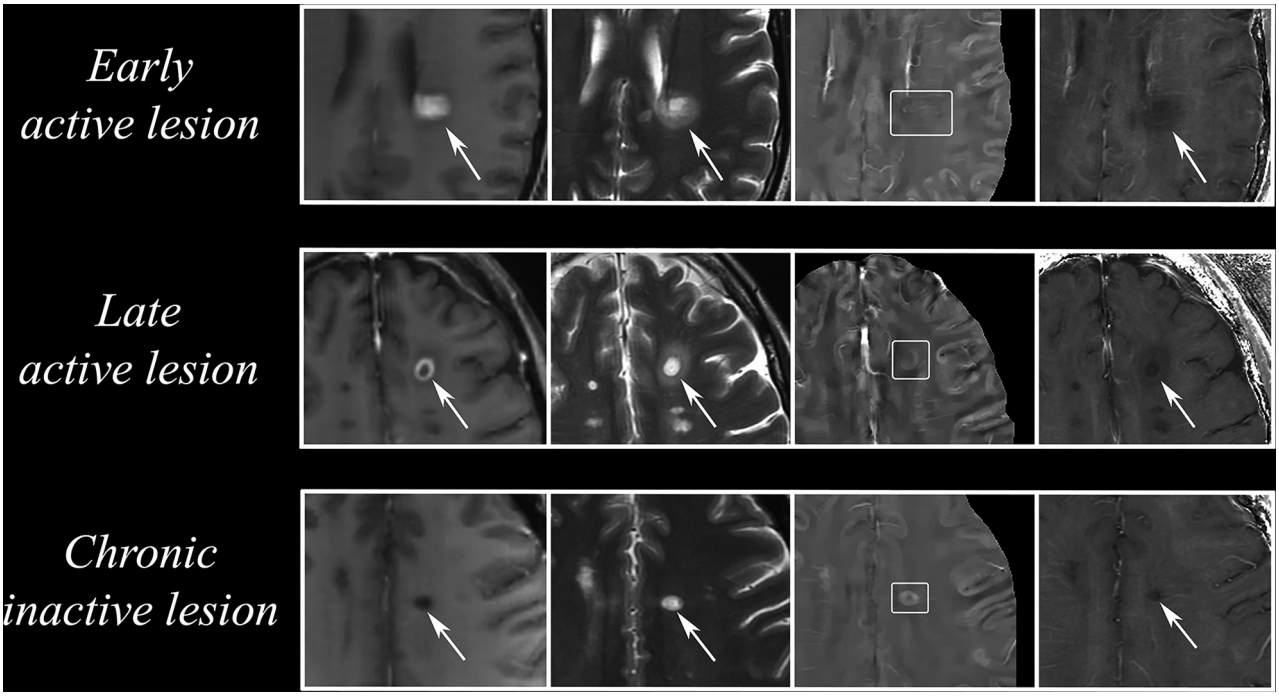

FIG 2. Conventional and quantitative MR imaging findings of WM lesions at different stages. In the *upper row*, conventional findings (postgadolinium T1-weighted and precontrast T2-weighted, *first and second images from left to right respectively*) of a typical pattern of nodular enhancement in an early active lesion (*arrows*) showing isointense signal in QSM (*third image*, *white box*) and mild hypointensity in R2* map (*fourth image*). In late active lesions (*middle row, arrows*), a peripheral pattern of enhancement is present, coupled with an area of increased signal at QSM and a slightly more pronounced hypointensity on R2* maps compared with the previous stage. As lesion staging further increases, the lesion eventually enters its chronic inactive stage (*lower row, arrows*), characterized by absent gadolinium enhancement, a QSM hyperintensity, and a hypointense R2* signal. Modified with permission from Zhang et al.[45]

cytokines produced by the chronically activated microglia,[14] with these mechanisms ultimately resulting in oxidative stress via Fenton chemistry and reduced regenerative capacity.[30]

Because these different microstructural changes influence multiple MR imaging contrasts contemporarily, multiparameter qMRI represents the most apt approach to explore pathologic alterations occurring in the MS brain. The undeniable advantage of qMRI relies on the possibility of generating spatial maps in which each voxel corresponds to a numeric value reflecting the physical properties of the examined tissues, such as free water proportion (PD, R1, R2), myelination (R1, R2, R2*, QSM), or iron content (R2* and QSM).[31,32]

While PD is an established measure of the brain free water pool,[33] with PD increase documented in the presence of vasogenic edema,[34] R1 and R2 vary as a function of free water and myelin concentration, with a higher degree of myelination causing relaxation time shortening.[35,36]

With reference to iron, in normal brain tissue, it is mostly bound to ferritin in oligodendrocytes,[37] and its presence is required for the activity of enzymes involved in myelin production and preservation.[15] Along with myelin, iron accounts for the larger part of the MR imaging contrast obtained through R2* and QSM.[38] However, whereas both iron and myelin determine an R2* increase, they play opposite roles in QSM. Given the paramagnetic properties of iron, an increase in its concentration is unequivocally coupled to an increase in susceptibility, while myelin, being a diamagnetic compound, influences susceptibility in the opposite direction.[38]

WM Lesions

Focal WM lesions represent the most typical expression of tissue damage in MS.[39] According to their activity phase, WM lesions can be histologically subcategorized as early active, late active, chronic active (also described as slowly expanding or smoldering lesions), chronic inactive, and shadow plaques (remyelinated lesions).[40]

In early active lesions, inflammatory activity blooms from venules, following blood-brain barrier disruption and immune cell infiltration, thus leading to progressive demyelination and axonal loss with a centrifugal spread.[41] From an MR imaging perspective, these phenomena are mirrored by the pattern of enhancement after gadolinium administration. Indeed, at this stage, lesions usually enhance centrifugally, with a more pronounced nodular appearance.[42] As inflammation proceeds, cellular infiltrates grow and, combined with myelin breaking down and edema, result in decreased R1 and R2 values, coupled to increased PD values within lesions[43] and transitional values in periplaque WM[44] in comparison with NAWM. These findings are associated with a similar edema-driven R2* decrease, with no QSM changes because the loss of diamagnetic myelin is not detectable at this stage (Fig 2).[45]

In late active lesions, showing a peripheral or ringlike pattern of enhancement,[42] myelin degradation and removal become progressively more substantial, therefore influencing lesion magnetic susceptibility as assessed by QSM.[45,46] At this stage, R1, R2, and PD values show the same pattern of changes as the early active lesions in comparison with NAWM, while in R2*, a further signal decrease is present, coupled to a QSM increase, especially in the lesion

Table 1: Major qMRI findings in MS—WM compartment

Site	Pathologic Processes and qMRI Correlates
WM lesions	
Early active	Decreased R1, R2, and R2* values, along with increased PD, reflecting initial myelin degradation and edema[43,45]
Late active	Decreased R1 and R2 values, coupled with increased PD, with myelin debris removal that determines further R2* decrease and QSM increase[43,45,51]
Chronic active	Further R1 and R2 decrease, with PD increase, due to demyelination progression;[43] increased R2* and QSM at the periphery of the lesions due to iron-laden microglia and macrophages[45,46]
Chronic inactive	Compared with chronic active, R2* decreases with high QSM values; across time, susceptibility values gradually become similar to those in NAWM[46]
NAWM	Decreased R1 and R2 values, with increased PD, compared with the WM of healthy controls,[50,51] reflecting edema and myelin loss secondary to inflammatory infiltration.
	During active phases of the disease, iron is released from oligodendrocytes and begins to accumulate in newly forming lesions, causing an R2* decrease[50] and no relevant modification of QSM signal[52]

center, due to additional myelin debris removal[45] by anti-inflammatory M2 macrophages.[14] Although iron begins concentrating in M1 macrophages and activated microglia at a later stage,[14] its levels may acutely increase following rapid oligodendrocyte destruction, counterbalancing myelin loss in R2* and reinforcing QSM hyperintensity in some lesions (Fig 2).[47]

When blood-brain barrier damage is resolved, MS lesions no longer show postgadolinium enhancement and are, therefore, categorized as chronic, further subdivided into active or inactive, depending on whether some degree of inflammatory activity persists.[40] In chronic lesions, the combination of demyelination, hypocellularity, and free water fraction increase leads to R1 and R2 decrease, while PD increases, compared with early and late active lesions.[43] Transition to chronicity is associated with a complex pattern of changes in iron content.[38] Indeed, while iron concentration may decrease due to myelin sheaths and oligodendrocyte depletion,[29,37] some degree of iron accumulation occurs, in parallel, within iron-laden macrophages and microglia at lesions borders.[14,32] In chronic active lesions, this inflammation-related iron accumulation at the rim of the lesions is emphasized, leading to increased R2* and QSM values.[45,46] With time, lesions eventually become chronic inactive or shadow plaques,[40] with low R2* values but still high QSM signal, which only ultimately decreases in very late stages to resemble NAWM signal, due to iron depletion and partial remyelination (Fig 2).[46]

NAWM

Despite appearing spared by lesions on conventional MR imaging sequences, NAWM is characterized by complex microstructural changes reflecting inflammation, demyelination, gliosis, and axonal loss.[28] The mechanisms underlying NAWM damage are mainly Wallerian degeneration of fibers transected by focal lesions and diffuse microglial activation.[28,48] Axonal swelling and edema[49] have also been observed globally in NAWM and, together with alteration in iron homeostasis, can be assessed through relaxation and magnetic susceptibility variations.[24,38]

The NAWM usually shows lower R1 and R2 and higher PD values, compared with the WM of healthy controls.[50,51] These changes seem to be mostly related to inflammatory infiltration, with edema and myelin loss.[49] A decrease in iron concentration has been observed in patients with MS in comparison with healthy controls using R2* maps.[50] This reduced relaxation rate might be driven by iron release from oligodendrocytes during chronic inflammation.[14,29] Most interesting, the iron level in NAWM, estimated by QSM, is not stationary but fluctuates according to the presence of inflammatory activity.[52] Indeed, during the active phases of the disease, when iron begins to accumulate in newly forming lesions, NAWM magnetic susceptibility values appear to be similar to those observed in the WM of healthy controls,[52] as also confirmed by ex vivo data.[29] On the contrary, mean QSM values of the NAWM seem to increase in the absence of gadolinium-enhancing lesions, suggesting that iron might play a role in tissue regeneration during periods of disease inactivity.[15]

Main qMRI findings in the WM compartment are reported in Table 1.

Deep Gray Matter

The major structures of the deep gray matter nuclei can be anatomically and functionally subdivided in the thalamus and basal ganglia, whose most relevant nuclei are the globus pallidus, putamen, and caudate nucleus. Given their relatively different histology, the thalamus and basal ganglia will be discussed separately.

Thalamus. Thalamic involvement in MS has been documented by both ex-[53-55] and in vivo[53] studies. This region is not only a site of primary axonal damage, but given its high interconnectivity with other brain regions, it suffers from secondary degeneration caused by WM lesions involving thalamic projection fibers.[53,54] Recently, a decrease in both thalamic iron content and concentration[56-61] has been documented in patients with MS in comparison with healthy controls, with the most evident changes detected within the pulvinar.[59,61]

Previous studies, however, reported conflicting results,[62-66] only partially ascribable to the physiologic nonlinear trajectory followed by thalamic iron concentration during the life span.[67] Such conflicting data should be interpreted considering the impact of atrophy on iron concentration.[57,68] In particular, the concept of R2* mass (the sum of all the R2* values in a specific region)[57] was recently introduced as an index of iron content independent of atrophy. With this approach, the decrease in thalamic iron content has been confirmed,[57] highlighting the importance of distinguishing between (and reporting both) iron concentration and content (Fig 3).[56,57,59,60]

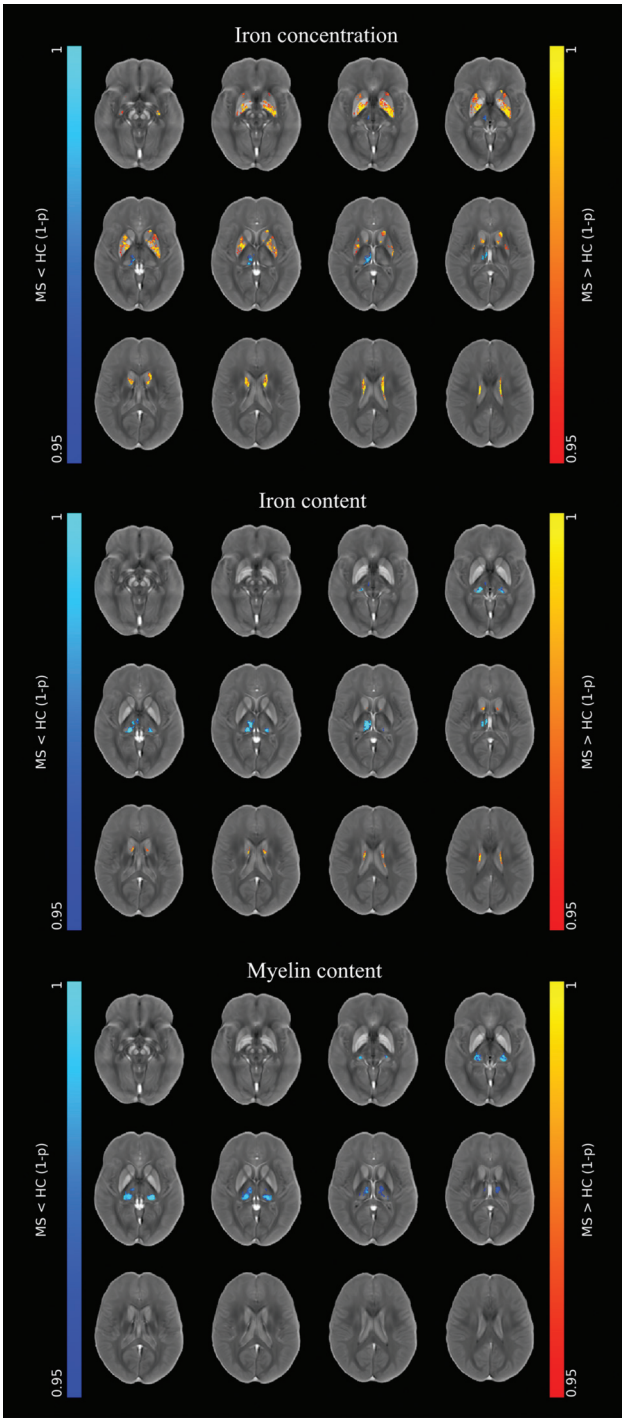

FIG 3. Pattern of iron concentration, iron content, and myelin content changes in deep gray matter nuclei in MS. Results of voxelwise analyses comparing patients with MS with healthy controls, showing the presence of an increased iron concentration at the level of the basal ganglia (red-yellow), coupled with a decrease in iron and myelin content mainly affecting the thalami and, in particular, the pulvinar nuclei (blue-light blue). Modified with permission from Pontillo et al.[59] HC indicates healthy control; 1-ρ, 1 minus *P* value.

Basal Ganglia. The basal ganglia are also the site of both demyelination[69] and neurodegeneration, with reduced neuronal density, axonal damage, and oligodendrocytes loss.[44,55]

Similar to what we described for the thalamus, the progressive damage of the basal ganglia leads to atrophy.[69] Here, studies have more consistently reported an increase in R2*[58,64-66,70,71] or susceptibility[61,64,66,70,72] in patients with MS compared with controls, suggesting a progressive iron accumulation, beyond the analogous physiologic process detectable in healthy individuals.[73]

Nonetheless, these findings should also be interpreted in view of the effect of atrophy on tissue iron concentration.[57] Indeed, even with stable regional iron content, volume reduction leads to increased mean iron concentration.[57] In particular, a prominent decline in iron content with time in all basal ganglia has been demonstrated, coupled with an increased or stable iron concentration compared with controls at the level of putamen, caudate nucleus, and globus pallidus.[60,72] In line with these results, some recent studies failed to identify any difference between patients with MS and controls in terms of iron content,[59] while others reported a decrease of this parameter in the putamen and caudate nucleus of patients with MS (Fig 3).[56,57]

Cortical Lesions

From a relaxometry perspective, no studies have investigated R1 changes in cortical lesions (CL). However, beyond demyelination, CL are characterized by a decreased iron load, a feature that allows differentiating them from a normal-appearing cortex through the evaluation of R2* maps, as shown in postmortem samples.[74,75] In particular, the progressive destruction of iron-rich myelin sheaths and oligodendrocytes[76] and the subsequent uptake of iron and myelin debris by activated macrophages and microglia lead to decreased R2* values in CL.[77] On the other hand, QSM has been used to analyze the heterogeneity of CL in different disease stages,[78] showing a mixed pattern of appearance. While QSM-hyperintense CL have been more frequently observed in patients with relapsing-remitting MS, QSM-hypointense CL are mostly identified in subjects with a secondary-progressive phenotype.[78] While the increased susceptibility might be due to iron release from oligodendrocytes, typical of the inflammatory phase of the disease, the reduced susceptibility might be linked to iron depletion in chronic lesions.[29]

Normal-Appearing Cortex

Similar to the NAWM, the cortex, which does not show signal changes on conventional MR imaging, is subject, from a pathologic standpoint, to neuronal and axonal loss occurring regardless of demyelination.[76,79] The assessment of relaxometry and QSM changes in normal-appearing cortex is confounded by the physiologic layer-specific iron content,[80] which represents the main source of cortical R2*[81] and susceptibility contrast.[36] Nevertheless, a decrease in both R1 and R2* values has been reported in MS in normal-appearing cortex, accounting for demyelination and iron depletion, respectively.[50] Consistent with the hypothesis of cortical demyelination triggered by chemokines produced by lymphocytic infiltrates in the meningeal compartment,[82] a recent study has reported coherent cortical gradients of R1 and R2*, oriented from the subpial layer to the WM interface.[83] In the same study, QSM showed a lack of sensitivity in distinguishing the different layers, probably due to the counteracting effects of diamagnetic myelin and paramagnetic iron modifications.[83]

Table 2: Major qMRI findings in MS—GM compartment

Site	Pathologic Processes and qMRI Correlates
Deep gray matter	
Basal ganglia	Increased R2*[58,64-66,70,71] and QSM values[61,64,66,70,72] indicating increased iron concentrations, with atrophy that might play a role in causing these changes[57,68]
Thalamus	The more recent findings suggest the presence of reduced iron content and concentration, along with demyelination, as shown by decreased R1, R2*, and QSM values[56-61]
Cortical gray matter	
Cortical lesions	Reduced R2* signal due to demyelination and iron depletion;[74,75] cortical lesions are more heterogeneous on QSM, with decreased-to-increased values, depending on the level of inflammatory activity[78]
Normal-appearing cortex	Demyelination and iron depletion lead to reduced R1 and R2* values,[50] with a gradient indicating the WM interface[83]

The main qMRI findings of the GM compartment are reported in Table 2.

CONCLUSIONS

In this review, we offered a comprehensive overview of qMRI applications in MS, while also describing the theory behind map generation and the most likely histologic correlates of qMRI findings. The multiparameter nature of qMRI has already allowed researchers to gain additional, valuable insights about the multifaceted pathophysiology of brain damage in MS. Given the increasing accessibility to quantitative sequences on novel MR imaging scanners, in the near future, qMRI will also likely play a fundamental role in clinical practice as a sensitive tool to quantitatively assess brain damage in patients with MS, with relevant implications for prognostic stratification and treatment-response evaluation.

Disclosure forms provided by the authors are available with the full text and PDF of this article at www.ajnr.org.

REFERENCES

1. Rovira À, Wattjes MP, Tintoré M, et al; MAGNIMS Study Group. **Evidence-based guidelines: MAGNIMS consensus guidelines on the use of MRI in multiple sclerosis-clinical implementation in the diagnostic process.** *Nat Rev Neurol* 2015;11:471–82 CrossRef Medline
2. Wattjes MP, Ciccarelli O, Reich DS, et al; North American Imaging in Multiple Sclerosis Cooperative MRI Guidelines Working Group. **MAGNIMS-CMSC-NAIMS consensus recommendations on the use of MRI in patients with multiple sclerosis.** *Lancet Neurol* 2021;20:653–70 CrossRef Medline
3. Hagiwara A, Otsuka Y, Andica C, et al. **Differentiation between multiple sclerosis and neuromyelitis optica spectrum disorders by multiparametric quantitative MRI using convolutional neural network.** *J Clin Neurosci* 2021;87:55–58 CrossRef Medline
4. Pudlac A, Burgetova A, Dusek P, et al. **Deep gray matter iron content in neuromyelitis optica and multiple sclerosis.** *BioMed Res Int* 2020;2020:6492786 CrossRef Medline
5. Deistung A, Schweser F, Reichenbach JR. **Overview of quantitative susceptibility mapping.** *NMR Biomed* 2017;30:e3569 CrossRef Medline
6. Seiler A, Nöth U, Hok P, et al. **Multiparametric quantitative MRI in neurological diseases.** *Front Neurol* 2021;12:640239 CrossRef Medline
7. Li J, Lin H, Liu T, et al. **Quantitative susceptibility mapping (QSM) minimizes interference from cellular pathology in R2* estimation of liver iron concentration.** *J Magn Reson Imaging* 2018;48:1069–79 CrossRef Medline
8. Banerjee R, Pavlides M, Tunnicliffe EM, et al. **Multiparametric magnetic resonance for the non-invasive diagnosis of liver disease.** *J Hepatol* 2014;60:69–77 CrossRef Medline
9. Straub S, Laun FB, Emmerich J, et al. **Potential of quantitative susceptibility mapping for detection of prostatic calcifications.** *J Magn Reson Imaging* 2017;45:889– 98 CrossRef Medline
10. Jerban S, Lu X, Jang H, et al. **Significant correlations between human cortical bone mineral density and quantitative susceptibility mapping (QSM) obtained with 3D cones ultrashort echo time magnetic resonance imaging (UTE-MRI).** *Magn Reson Imaging* 2019;62:104–10 CrossRef Medline
11. Karur GR, Hanneman K. **Cardiac MRI T1, T2, and T2* mapping in clinical practice.** *Advances in Clinica Radiology* 2019;1:27–41 CrossRef
12. Granziera C, Wuerfel J, Barkhof F, et al; MAGNIMS Study Group. **Quantitative magnetic resonance imaging towards clinical application in multiple sclerosis.** *Brain* 2021;144:1296–1311 CrossRef Medline
13. Pontillo G, Cocozza S, Lanzillo R, et al. **Determinants of deep gray matter atrophy in multiple sclerosis: a multimodal MRI study.** *AJNR Am J Neuroradiol* 2019;40:99–106 CrossRef Medline
14. Mehta V, Pei W, Yang G, et al. **Iron is a sensitive biomarker for inflammation in multiple sclerosis lesions.** *PLoS One* 2013;8:e57573 CrossRef Medline
15. Möller HE, Bossoni L, Connor JR, et al. **Iron, myelin, and the brain: neuroimaging meets neurobiology.** *Trends Neurosci* 2019;42:384–401 CrossRef Medline
16. Deoni SC, Rutt BK, Peters TM. **Rapid combined T1 and T2 mapping using gradient recalled acquisition in the steady state.** *Magn Reson Med* 2003;49:515–26 CrossRef Medline
17. Yarnykh VL. **Actual flip-angle imaging in the pulsed steady state: a method for rapid three-dimensional mapping of the transmitted radiofrequency field.** *Magn Reson Med* 2007;57:192–200 CrossRef Medline
18. Palma G, Tedeschi E, Borrelli P, et al. **A novel multiparametric approach to 3D quantitative MRI of the brain.** *PLoS One* 2015;10:e0134963 CrossRef Medline
19. Baudrexel S, Nöth U, Schüre JR, et al. **T_1 mapping with the variable flip angle technique: a simple correction for insufficient spoiling of transverse magnetization.** *Magn Reson Med* 2018;79:3082–92 CrossRef Medline
20. Björk M, Ingle RR, Gudmundson E, et al. **Parameter estimation approach to banding artifact reduction in balanced steady-state free precession.** *Magn Reson Med* 2014;72:880–92 CrossRef Medline
21. Monti S, Borrelli P, Tedeschi E, et al. **RESUME: turning an SWI acquisition into a fast qMRI protocol.** *PLoS One* 2017;12:e0189933 CrossRef Medline
22. Monti S, Pontillo G, Russo C, et al. **RESUME^N: a flexible class of multi-parameter qMRI protocols.** *Phys Med* 2021;88:23–36 CrossRef Medline
23. Li W, Wang N, Yu F, et al. **A method for estimating and removing streaking artifacts in quantitative susceptibility mapping.** *Neuroimage* 2015;108:111–22 CrossRef Medline
24. Li W, Wu B, Liu C. **Quantitative susceptibility mapping of human brain reflects spatial variation in tissue composition.** *Neuroimage* 2011;55:1645–56 CrossRef Medline
25. Aja-Fernández S, Pieciak T, Vegas-Sánchez-Ferrero G. **Spatially variant noise estimation in MRI: a homomorphic approach.** *Med Image Anal* 2015;20:184–97 CrossRef Medline

26. Borrelli P, Palma G, Tedeschi E, et al. **Improving signal-to-noise ratio in susceptibility weighted imaging: a novel multicomponent non-local approach.** *PLoS One* 2015;10:e0126835 CrossRef Medline
27. Filippi M, Bar-Or A, Piehl F, et al. **Multiple sclerosis.** *Nat Rev Dis Primers* 2018;4:43 CrossRef Medline
28. Allen IV, McQuaid S, Mirakhur M, et al. **Pathological abnormalities in the normal-appearing white matter in multiple sclerosis.** *Neurolo Sci* 2001;22:141–44 CrossRef Medline
29. Hametner S, Wimmer I, Haider L, et al. **Iron and neurodegeneration in the multiple sclerosis brain.** *Ann Neurol* 2013;74:848–61 CrossRef Medline
30. Stephenson E, Nathoo N, Mahjoub Y, et al. **Iron in multiple sclerosis: roles in neurodegeneration and repair.** *Nat Rev Neurol* 2014;10:459–68 CrossRef Medline
31. Weiskopf N, Edwards LJ, Helms G, et al. **Quantitative magnetic resonance imaging of brain anatomy and in vivo histology.** *Nat Rev Phys* 2021;3:570–88 CrossRef
32. Wisnieff C, Ramanan S, Olesik J, et al. **Quantitative susceptibility mapping (QSM) of white matter multiple sclerosis lesions: Interpreting positive susceptibility and the presence of iron.** *Magn Reson Med* 2015;74:564–70 CrossRef Medline
33. Tofts PS. PD: proton density of tissue water. In: Tofts PS. *Quantitative MRI of the Brain: Measuring Changes Caused by Disease*. Wiley Online Library; 2003:85–109
34. Eis M, Els T, Hoehn-Berlage M. **High resolution quantitative relaxation and diffusion MRI of three different experimental brain tumors in rat.** *Magn Reson Med* 1995;34:835–44 CrossRef Medline
35. Schmierer K, Wheeler-Kingshott CA, Tozer DJ, et al. **Quantitative magnetic resonance of postmortem multiple sclerosis brain before and after fixation.** *Magn Reson Med* 2008;59:268–77 CrossRef Medline
36. Stüber C, Morawski M, Schäfer A, et al. **Myelin and iron concentration in the human brain: a quantitative study of MRI contrast.** *Neuroimage* 2014;93 Pt 1:95–106 CrossRef Medline
37. Bagnato F, Hametner S, Yao B, et al. **Tracking iron in multiple sclerosis: a combined imaging and histopathological study at 7 Tesla.** *Brain* 2011;134:3602–15 CrossRef Medline
38. Hametner S, Endmayr V, Deistung A, et al. **The influence of brain iron and myelin on magnetic susceptibility and effective transverse relaxation: a biochemical and histological validation study.** *Neuroimage* 2018;179:117–33 CrossRef Medline
39. van der Valk P, De Groot CJ. **Staging of multiple sclerosis (MS) lesions: pathology of the time frame of MS.** *Neuropathol Appl Neurobiol* 2000;26:2–10 CrossRef Medline
40. Frischer JM, Weigand SD, Guo Y, et al. **Clinical and pathological insights into the dynamic nature of the white matter multiple sclerosis plaque.** *Ann Neurol* 2015;78:710–21 CrossRef Medline
41. Tallantyre EC, Brookes MJ, Dixon JE, et al. **Demonstrating the perivascular distribution of MS lesions in vivo with 7-Tesla MRI.** *Neurology* 2008;70:2076–78 CrossRef Medline
42. Gaitán MI, Shea CD, Evangelou IE, et al. **Evolution of the blood-brain barrier in newly forming multiple sclerosis lesions.** *Ann Neurol* 2011;70:22–29 CrossRef Medline
43. Blystad I, Håkansson I, Tisell A, et al. **Quantitative MRI for analysis of active multiple sclerosis lesions without gadolinium-based contrast agent.** *AJNR Am J Neuroradiol* 2016;37:94–100 CrossRef Medline
44. Hagiwara A, Hori M, Yokoyama K, et al. **Utility of a multiparametric quantitative MRI model that assesses myelin and edema for evaluating plaques, periplaque white matter, and normal-appearing white matter in patients with multiple sclerosis: a feasibility study.** *AJNR Am J Neuroradiol* 2017;38:237–42 CrossRef Medline
45. Zhang Y, Gauthier SA, Gupta A, et al. **Quantitative susceptibility mapping and R2* measured changes during white matter lesion development in multiple sclerosis: myelin breakdown, myelin debris degradation and removal, and iron accumulation.** *AJNR Am J Neuroradiol* 2016;37:1629–35 CrossRef Medline
46. Chen W, Gauthier SA, Gupta A, et al. **Quantitative susceptibility mapping of multiple sclerosis lesions at various ages.** *Radiology* 2014;271:183–92 CrossRef Medline
47. Harrison DM, Li X, Liu H, et al. **Lesion heterogeneity on high-field susceptibility MRI is associated with multiple sclerosis severity.** *AJNR Am J Neuroradiol* 2016;37:1447–53 CrossRef Medline
48. Dziedzic T, Metz I, Dallenga T, et al. **Wallerian degeneration: a major component of early axonal pathology in multiple sclerosis.** *Brain Pathol* 2010;20:976–85 CrossRef Medline
49. Filippi M, Rocca MA, Barkhof F, et al; Attendees of the Correlation between Pathological MRI Findings in MS Workshop. **Association between pathological and MRI findings in multiple sclerosis.** *Lancet Neurol* 2012;11:349–60 CrossRef Medline
50. Lommers E, Simon J, Reuter G, et al. **Multiparameter MRI quantification of microstructural tissue alterations in multiple sclerosis.** *Neuroimage Clin* 2019;23:101879 CrossRef Medline
51. West J, Aalto A, Tisell A, et al. **Normal-appearing and diffusely abnormal white matter in patients with multiple sclerosis assessed with quantitative MR.** *PLoS One* 2014;9:e95161 CrossRef Medline
52. Chen W, Zhang Y, Mu K, et al. **Quantifying the susceptibility variation of normal-appearing white matter in multiple sclerosis by quantitative susceptibility mapping.** *AJR Am J Roentgenol* 2017;209:889–94 CrossRef Medline
53. Cifelli A, Arridge M, Jezzard P, et al. **Thalamic neurodegeneration in multiple sclerosis.** *Ann Neurol* 2002;52:650–53 CrossRef Medline
54. Mahajan KR, Nakamura K, Cohen JA, et al. **Intrinsic and extrinsic mechanisms of thalamic pathology in multiple sclerosis.** *Ann Neurol* 2020;88:81–92 CrossRef Medline
55. Vercellino M, Masera S, Lorenzatti M, et al. **Demyelination, inflammation, and neurodegeneration in multiple sclerosis deep gray matter.** *J Neuropathol Exp Neurol* 2009;68:489–502 CrossRef Medline
56. Elkady AM, Cobzas D, Sun H, et al. **Five year iron changes in relapsing-remitting multiple sclerosis deep gray matter compared to healthy controls.** *Mult Scler Relat Disord* 2019;33:107–15 CrossRef Medline
57. Hernández-Torres E, Wiggermann V, Machan L, et al. **Increased mean R2* in the deep gray matter of multiple sclerosis patients: have we been measuring atrophy?** *J Magn Reson Imaging* 2019;50:201–08 CrossRef Medline
58. Khalil M, Langkammer C, Pichler A, et al. **Dynamics of brain iron levels in multiple sclerosis: a longitudinal 3T MRI study.** *Neurology* 2015;84:2396–2402 CrossRef Medline
59. Pontillo G, Petracca M, Monti S, et al. **Unraveling deep gray matter atrophy and iron and myelin changes in multiple sclerosis.** *AJNR Am J Neuroradiol* 2021;42:1223–30 CrossRef Medline
60. Schweser F, Hagemeier J, Dwyer MG, et al. **Decreasing brain iron in multiple sclerosis: the difference between concentration and content in iron MRI.** *Hum Brain Mapp* 2021;42:1463–74 CrossRef Medline
61. Zivadinov R, Tavazzi E, Bergsland N, et al. **Brain iron at quantitative MRI is associated with disability in multiple sclerosis.** *Radiology* 2018;289:487–96 CrossRef Medline
62. Cobzas D, Sun H, Walsh AJ, et al. **Subcortical gray matter segmentation and voxel-based analysis using transverse relaxation and quantitative susceptibility mapping with application to multiple sclerosis.** *J Magn Reson Imaging* 2015;42:1601–10 CrossRef Medline
63. Lebel RM, Eissa A, Seres P, et al. **Quantitative high-field imaging of sub-cortical gray matter in multiple sclerosis.** *Mult Scler* 2012;18:433–41 CrossRef Medline
64. Rudko DA, Solovey I, Gati JS, et al. **Multiple sclerosis: improved identification of disease-relevant changes in gray and white matter by using susceptibility-based MR imaging.** *Radiology* 2014;272:851–64 CrossRef Medline
65. Walsh AJ, Blevins G, Lebel RM, et al. **Longitudinal MR imaging of iron in multiple sclerosis: an imaging marker of disease.** *Radiology* 2014;270:186–96 CrossRef Medline
66. Fujiwara E, Kmech JA, Cobzas D, et al. **Cognitive implications of deep gray matter iron in multiple sclerosis.** *AJNR Am J Neuroradiol* 2017;38:942–48 CrossRef Medline
67. Hallgren B, Sourander P. **The effect of age on the non-haemin iron in the human brain.** *Neurochem* 1958;3:41–51 CrossRef Medline

68. Eshaghi A, Marinescu RV, Young AL, et al. **Progression of regional grey matter atrophy in multiple sclerosis.** *Brain* 2018;141:1665–77 CrossRef Medline
69. Haider L, Simeonidou C, Steinberger G, et al. **Multiple sclerosis deep grey matter: the relation between demyelination, neurodegeneration, inflammation and iron.** *J Neurol Neurosurg Psychiatry* 2014;85:1386–95 CrossRef Medline
70. Elkady AM, Cobzas D, Sun H, et al. **Progressive iron accumulation across multiple sclerosis phenotypes revealed by sparse classification of deep gray matter.** *J Magn Reson Imaging* 2017;46:1464–73 CrossRef Medline
71. Ropele S, Kilsdonk ID, Wattjes MP, et al. **Determinants of iron accumulation in deep grey matter of multiple sclerosis patients.** *Mult Scler* 2014;20:1692–98 CrossRef Medline
72. Hagemeier J, Zivadinov R, Dwyer MG, et al. **Changes of deep gray matter magnetic susceptibility over 2 years in multiple sclerosis and healthy control brain.** *Neuroimage Clin* 2018;18:1007–16 CrossRef Medline
73. Haacke EM, Cheng NY, House MJ, et al. **Imaging iron stores in the brain using magnetic resonance imaging.** *Magn Reson Imaging* 2005;23:1–25 CrossRef Medline
74. Jonkman LE, Fleysher L, Steenwijk MD, et al. **Ultra-high field MTR and qR2* differentiates subpial cortical lesions from normal-appearing gray matter in multiple sclerosis.** *Mult Scler* 2016;22:1306–14 CrossRef Medline
75. Yao B, Hametner S, van Gelderen P, et al. **7 Tesla magnetic resonance imaging to detect cortical pathology in multiple sclerosis.** *PLoS One* 2014;9:e108863 CrossRef Medline
76. Peterson JW, Bö L, Mörk S, et al. **Transected neurites, apoptotic neurons, and reduced inflammation in cortical multiple sclerosis lesions.** *Ann Neurol* 2001;50:389–400 CrossRef Medline
77. Fischer MT, Wimmer I, Höftberger R, et al. **Disease-specific molecular events in cortical multiple sclerosis lesions.** *Brain* 2013;136:1799–1815 CrossRef Medline
78. Castellaro M, Magliozzi R, Palombit A, et al. **Heterogeneity of cortical lesion susceptibility mapping in multiple sclerosis.** *AJNR Am J Neuroradiol* 2017;38:1087–95 CrossRef Medline
79. Magliozzi R, Howell OW, Reeves C, et al. **A Gradient of neuronal loss and meningeal inflammation in multiple sclerosis.** *Ann Neurol* 2010;68:477–93 CrossRef Medline
80. Fukunaga M, Li TQ, van Gelderen P, et al. **Layer-specific variation of iron content in cerebral cortex as a source of MRI contrast.** *Proc Natl Acad Sci U S A* 2010;107:3834–39 CrossRef Medline
81. Bagnato F, Hametner S, Boyd E, et al. **Untangling the R2* contrast in multiple sclerosis: a combined MRI-histology study at 7.0 Tesla.** *PLoS One* 2018;13:e0193839 CrossRef Medline
82. Magliozzi R, Reynolds R, Calabrese M. **MRI of cortical lesions and its use in studying their role in MS pathogenesis and disease course.** *Brain Pathol* 2018;28:735–42 CrossRef Medline
83. Lema Dopico A, Choi S, Hua J, et al. **Multi-layer analysis of quantitative 7 T magnetic resonance imaging in the cortex of multiple sclerosis patients reveals pathology associated with disability.** *Mult Scler* 2021;27:2040–51 CrossRef Medline